Insights into the Mechanism of Binding of Arachidonic Acid to Mammalian 15-Lipoxygenases

Lea Toledo,[†] Laura Masgrau,*[,‡] Jean-Didier Maréchal,[†] José M. Lluch,[†,‡] and Àngels González-Lafont*[,†,‡]

Departament de Química and Institut de Biotecnologia i de Biomedicina (IBB), Universitat Autònoma de Barcelona, 08193 Bellaterra, Barcelona, Spain

Received: December 23, 2009; Revised Manuscript Received: March 23, 2010

Mammalian 15-lipoxygenases (15-LOs) are key pharmaceutical targets under strong investigation because of their implication in atherosclerosis and cancer. Here, we present an atomic-level study of the binding modes of arachidonic acid (AA) to rabbit reticulocyte 15-LO, with a particular insight into the 15-LO:AA complexes consistent with known catalytic activity. We take into account both ligand and protein flexibility, by combining protein−ligand docking techniques and molecular dynamics simulations. We have also performed in silico mutagenesis. Our results are in agreement with previous mutagenesis data, in particular with the importance of Arg403 on AA binding. Interestingly, our results also reveal a central role of Arg403 in the conformational change of the α2-helix observed upon ligand binding. That induced-fit effect could give a possible framework for the molecular explanation of the known allosteric effect and questions the suitability of the inhibitor-bound crystal structure for accepting AA. Accounting for these dynamical considerations might improve the drug design process.

Introduction

Lipoxygenases (LOs) are present in a wide variety of organisms, including mammals, plants, and bacteria.[1,2] They are vital enzymes for the regulation of metabolic processes[3] but have also been related to the pathogenesis of several diseases. LOs are nonheme iron-containing enzymes that catalyze the stereospecific hydroperoxidation of polyunsaturated fatty acids containing 1,4-*cis*,*cis*-pentadiene. An in depth understanding of the catalytic activity of an enzyme may prove very valuable for the rational design of inhibitors. For this reason, an important research effort is being made by several groups in an attempt to better understand the molecular details of LOs substrate recognition, allostery, and catalytic mechanism.[4–13] The generally accepted mechanism proceeds by an initial hydrogen atom abstraction from the central carbon of the pentadiene moiety by the Fe(III)−OH^- cofactor, forming a substrate radical and Fe(II)−OH_2 (Scheme 1).[14–17] Both experimental and theoretical works have demonstrated that this H-abstraction involves hydrogen tunneling.[13,18–20] However, mechanistic differences have been reported in LOs with different substrates, even though hydrogen atom tunneling could be a common mechanistic feature.[10,12,13,21] Molecular oxygen, which is thought to reach the active site via defined channels,[6,22,23] reacts with the resulting radical giving the hydroperoxide product and regenerating the enzyme catalytic machinery.

Mammalian LOs have dual catalytic specificity with the same substrate or different catalytic specificity, depending on the substrate. In the case of 15-LOs, human reticulocyte 15-LO (15-hLO) catalyzes the hydroperoxidation of arachidonic acid (AA, its native substrate) (Scheme 1) to 15*S*-hydroperoxy-5*Z*,8*Z*,11*Z*,13*E*-eicosatetraenoic acid (15*S*-HPETE), but it also produces small amounts of 12*S*-HPETE (with a 15:12 ratio of ∼90:10).[12,24] The rabbit counterpart (15-rLO) shows a higher regiospecificity (ratio of 97:3).[25] Catalytic regio- and stereospecificity of enzymes depend on several factors, one of the most important being the binding mode of the ligand into the catalytic site.[26]

SCHEME 1: Reaction Mechanism of AA Hydroperoxidation by 15-LO

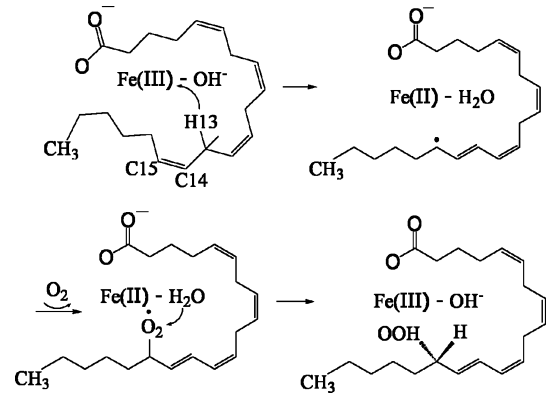

Before structural data on LOs were available, it was shown by comparing different LOs isoforms, mutagenesis experiments, and modeling studies that amino acids at the bottom of the putative substrate-binding cavity could determine the shape and the volume of the pocket and, therefore, be used by the enzyme to modulate regiospecificity.[27–29] In the case of 15-hLO, an important role for Arg402 as another determinant of substrate positional specificity was also shown.[24] Those experiments led to a certain consensus in 15-LOs about AA binding with its methyl end first. With the publication in the Protein Data Bank of the first 15-rLO X-ray crystallographic structure (PDB access code: 1LOX), the LO substrate binding site was inferred by the position of a bound inhibitor (RS7), and it was described

* To whom correspondence should be addressed. (A.G.-L.) Tel: +(34)935811672. Fax: +(34)935812920. E-mail: angels@klingon.uab.es. (L.M.) Tel: +(34)935868937. Fax: +(34)935812011. E-mail: laura.masgrau@uab.cat.

[†] Departament de Química.

[‡] Institut de Biotecnologia i de Biomedicina (IBB).

10.1021/jp912120n © 2010 American Chemical Society
Published on Web 04/30/2010

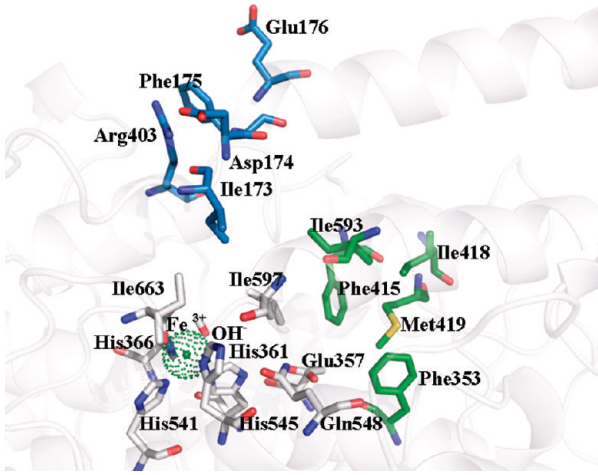

Figure 1. Representation of the binding site of rabbit reticulocyte 15-LO showing the iron coordination and the most important residues. Hydrogen atoms are not shown for clarity. The iron atom with its five protein ligands (His361, His366, His541, His545, and C-terminal Ile663) is located in the core of the catalytic domain.

as a boot-shaped hydrophobic pocket within the C-terminal domain directly accessible from the enzyme surface (Figure 1).[30,31] AA was modeled into this deep hydrophobic pocket with the methyl end extending down into the bottom of the pocket and the carboxylate end tethered on the surface of the enzyme by Arg403. This model of substrate binding provided a unifying hypothesis for the positional specificity of mammalian LOs. For 15-rLO, residues Arg403, Ile418, Phe353, and Ile593 (and Met419 to a less extent) have been confirmed by mutagenesis experiments to be determinant of positional specificity, probably by interacting with the methyl end of AA, except Arg403, which would interact with the carboxylate of AA (the kinetic experiments for the Arg403Leu mutant were performed with linoleic acid as a substrate instead of AA).[25,32] However, it has also been proposed that different substrates could bind in opposite orientations (methyl end or carboxylate end first) to control the site of oxygenation.[32]

In 2007, the original X-ray data were reinterpreted, leading to a new set of Cartesian coordinates for 15-rLO (PDB access code: 2P0M).[33] In this newly released structure, the ligand-bound monomer displays a closed conformation with the α2-helix blocking the entrance to the active site, while the ligand-free enzyme displays an open conformation with the entrance wide open but with a shallow pocket. The general form of the active site of this new X-ray structure represents an alternative to the cavity considered in previous works. As the authors point out, the shape of the cavity in the 2P0M structure suggests that AA may bind in a horseshoe-like conformation, assuming that this closed conformation of the enzyme is productive. Therefore, modeling of a 15-LO:AA complex should include protein and ligand flexibility. In this respect, it is worth mentioning that Kuhn et al.[5] have recently carried out dynamic fluorescence measurements to study temperature-induced conformational changes arising from three-dimensional fluctuations of the 15-rLO protein matrix. Those experiments have indicated that the rabbit enzyme exhibits a higher degree of conformational flexibility of the entire protein (global flexibility) and offers the possibility of augmented AA movement at the catalytic center (local flexibility) in comparison with the soybean enzyme. Moreover, effector-bound allosteric effects have also been observed in LOs.[34–36] In particular, Holman et al.[11] have recently shown how the binding of an effector molecule (LO product) to an allosteric site in 15-hLOs can change substrate specificity, pointing to an autoregulatory mechanism that could involve different LOs. The allosteric effector also changes the nature of the rate-limiting contributions of the individual steps in the catalytic mechanism. According to the authors, that structural mobility in 15-hLO may have relevance with respect to substrate specificity and recognition, but the lack of knowledge of the detailed structural features of the 15-hLO:AA complex prevented a deeper understanding.

Despite the intensive work devoted to LOs, several key questions remain unanswered, in particular, the binding mode of AA in a configuration ready for catalysis and how molecular flexibility affects the catalytic process. In this work, we present a molecular modeling study of the complexation of reticulocyte 15-rLO (the only mammalian 15-LO for which the three-dimensional structure is available) with its native substrate AA, with a particular insight into complexes consistent with known catalytic activity (precatalytic complexes) and taking into account both ligand and protein flexibility. We used a combination of protein−ligand docking techniques with molecular dynamics (MD) simulations. The different possible binding modes found in our study are discussed in light of the available mutagenesis data and general molecular knowledge on catalytic specificity.

Computational and Simulation Details

The strategy applied in this work represents a current state-of-the-art approach for dealing with protein−ligand dockings in flexible receptors[37–42] but with the particularity of focusing on the search of catalytically active complexes and not on inhibition properties. The general protocol can be briefly summarized as follows. First, protein−ligand dockings were applied to generate 15-rLO:AA complexes. Analysis of these results led to the selection of several possible enzyme:substrate precatalytic structures. They were used as the starting point for four independent MD simulations, which allow the relaxation of the whole solvated enzyme:substrate complex. To assess the effect of protein flexibility in the docking calculations and to see if the results got enriched with precatalytic complexes, a redocking of AA was carried out with nine protein structures taken from the MD simulations. These results were used to analyze the suitability of the available crystal structure for accepting the natural ligand and to discuss the effect of the induced fit as simulated in our approach. Finally, in silico mutagenesis was performed for Arg403 to further investigate the role of this residue in AA binding. In this section, we will describe the details of the calculations.

Docking Calculations. Protein−ligand dockings were performed with the AutoDock program version 4.0 with rigid side chains.[43,44] The coordinates for the receptor were taken from the closed monomer of the 2P0M crystal structure (chain B).[33] For the setup of the receptor, an oxidation state of III was assigned to the iron, as it is in the active form of the enzyme, and the hydroxide anion was modeled (Scheme 1). The protonation state of the ionizable residues was determined with the PROPKA program as well as by visual inspection.[45,46] The protein and ligand structures were prepared with AutoDock Tools.[47] For the standard atoms, the Kollman united-atom partial charges were used.[48] As these charges are not defined for the iron and its coordination environment, partial charges derived from quantum mechanics electronic structure calculations were assigned to these atoms. To this aim, a model cluster of the Fe^{3+} and its coordination sphere was energy minimized at the M05/LANL2DZ level of theory.[49–51] The model consisted of the iron atom, the OH^-, the isoleucine residue, and four

imidazole rings. A natural population analysis (NPA)[52] was carried out. The calculated NPA charges (1.365 au for Fe, −0.910 au for O, and 0.524 au for H) were assigned to the iron and the hydroxide ion. The remaining excess charge needed to fulfill the classical charge of +1 for the iron, and its first coordination sphere was distributed among the rest of the coordinating atoms.

For the ligand, the Kollman united-atom partial charges were used. A total of 14 torsional bonds were allowed to rotate during the docking process. The grid maps were calculated using AutoGrid4.0, with 126 × 106 × 126 points and a grid point spacing of 0.153 Å. These values were chosen so that the whole active site, which is quite big, was considered in the calculations.

The docking calculations were run with the Lamarckian Genetic Algorithm[44] in Autodock4.0, which combines a genetic algorithm and an adaptative local search algorithm. A total of 100 runs were launched. Most of the parameters for the genetic algorithm were set to the default values recommended by the program, except for the maximum number of energy evaluations and generations, which were set to larger values (2.5×10^6 and 2.7×10^5, respectively) to account for the degrees of freedom of the system under study and were at the limit of the combinatorial explosion.

MD Simulations. From the analysis of the docking results, four 15-rLO:AA models were selected. The crystallographic water molecules were added to the enzyme:substrate complex, and the missing hydrogens were built with the HBUILD facility in CHARMM.[53,54] The system was then solvated with a 117 Å × 82 Å × 70 Å box of preequilibrated TIP3P waters. The total charge of the system was neutralized with the addition of seven sodium cations. The resulting solvated enzyme:substrate complex had a total of ∼72100 atoms, with ∼10600 of them belonging to the 663 residue protein. The system was submitted to some energy minimization steps. MD simulations under periodic boundary conditions (PBCs) were then started. The system was gradually heated from 20 to 298 K in a time period of 365 ps, followed by a trajectory of 300 ps to ensure equilibration. During the heating and the first part of the equilibration, restraints were applied to the protein and the ligand. In particular, the C13−OH^- distance [*d*(C13−OH)] was restrained to the corresponding value obtained in the docking solution. Those restraints were gradually released, and a production period of 2 ns was run. From the analysis of those initial MD calculations, a 15rLO:AA model was selected, and three independent 4 ns trajectories were completed. Overall, 18 ns of the enzyme:substrate system was simulated. All of the simulations were done at constant pressure and temperature (CPT), using the extended system constant pressure and the Hoover constant temperature algorithms.[55] A time step of 2 fs was used. All of the angles and bonds involving hydrogen atoms were constrained by the SHAKE algorithm.[56] The PBCs were built with the CRYSTAL module of CHARMM using an orthorhombic unit cell. The Particle Mesh Ewald method for long-range electrostatics was used.

All of the MD simulations were run with CHARMM version c35. The force field topology and parameters for the AA ligand were derived from the lipids CHARMM-27 ones.[57,58] The CHARMM-22 force field parameters[59,60] were used for the protein atoms, but for the iron and its first coordination sphere, we used the parameters specifically developed by Saam et al.[6] for this system. Structural analysis of the simulations was performed with the CORREL module in CHARMM.

Redocking to Several Enzyme Structures. A total of nine 15-rLO:AA representative structures from the MD simulations were selected for redocking AA. This is an approach used in docking calculations to account in some way for the protein flexibility. In all of the selected structures, the C13−OH^- distance is suitable for hydrogen abstraction. The redocking was done as described above but adapting the grid parameters to the new conformations so that all of the important residues were taken into account in the calculations.

In Silico Mutagenesis. Mutants of Arg403 (to Ala, Leu, and Lys) were generated in silico for the nine structures used in the redocking. This was done with the program Chimera,[61] by changing the residue side chain and searching for the best rotamer in each case. The mutants were used for a new docking of AA, following the same procedure described above.

Results

Docking Calculations. The 100 models of the 15-rLO:AA complex produced by the docking calculations have predicted binding energies ranging from −7.24 to −5.09 kcal mol^{-1}. In low-energy complexes, the carboxylate end of AA interacts with different polar residues of the protein or with the Fe^{3+}−OH^- cofactor. In particular, the lowest energy model presents a hydrogen bond between the AA carboxylate and the Arg403, in agreement with the experimental mutagenesis studies with linoleic acid as a substrate. Interestingly, in the second lowest energy model (−6.76 kcal mol^{-1}), the AA is bound in an inverted orientation, with the AA carboxylate hydrogen bonded to Gln548, a residue participating in a network of hydrogen bonds between the first and the second iron coordination spheres.[20,62]

For further analysis, a first structural clustering was done with an rmsd cutoff of 3.0 Å (see the Supporting Information, Figure S1). A total of 27 clusters were obtained. However, for the purpose of this work, we have regrouped the clusters in five families. The classification has been done according to the position of the carboxylate group of AA. Figure 2 shows a representation of these families, together with a depiction of a cut of the active site cavity. It is clear that most of the models found by the docking calculations (families F3 and F5) match the shape of the major pocket present in the 15-rLO active site. Only three families of docking solutions (F1, F4, and F5) display the AA carboxylate−Arg403 interaction experimentally reported as crucial for AA binding and substrate positional specificity in 15-hLO. In the case of F5, the AA is also close to the residues at the bottom of the cavity that are thought to be in close contact with AA (Ile593, Ile418, Met419, and Phe353). This is also the case for some models in F4. However, for F1, AA is bound less deep into the cavity and far from these residues. The other two families (F3 and F2) do not present the AA carboxylate−Arg403 interaction.

In terms of the distance of C13 to the hydroxyl oxygen (donor carbon and acceptor oxygen in the hydrogen-transfer reaction, Scheme 1), there are six models out of the 100 calculated with *d*(C13−OH) < 3.5 Å and 36 with *d*(C13−OH) < 4.5 Å that would be an acceptable distance for hydrogen-transfer reaction to be plausible. Most of these models belong to F1, although F4 and F5 also have models with C13−OH^- distances below 4.5 Å. Interestingly, there is a considerable number of models with a short C10−OH^- distance (68 below 4.5 Å). This result will be discussed in the next section.

Initial MD Simulations of the 15-rLO:AA Complex. MD simulations were performed on three models taken from the docking calculations. These models were selected based on the *d*(C13−OH) distance and the presence of the interaction of the AA carboxylate with Arg403. The positioning of the methyl

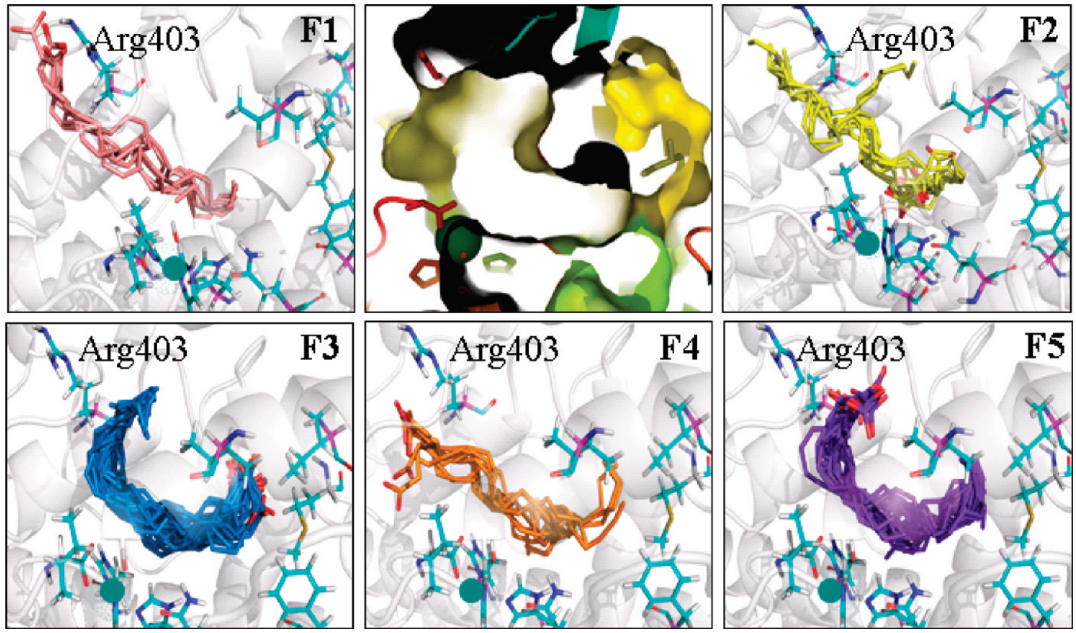

Figure 2. Structural families (F1−F5) in which the docking results have been regrouped according to the position of the carboxylate of AA, together with a depiction of the binding site cavity. The iron is depicted as a green sphere.

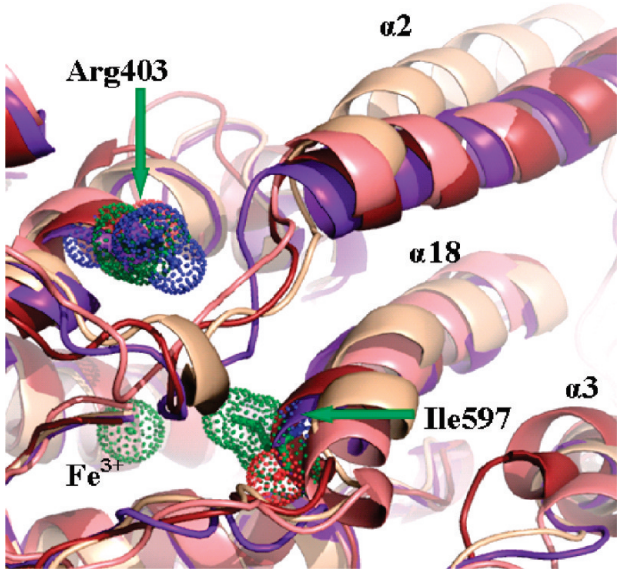

Figure 3. Superposition of representative 15-rLO:AA complexes from the 2 ns MD simulations of the M-F1 (brown), M-F4 (beige), and M-F5 (pink) models. The ligand-bound crystal structure is also depicted (violet), with Arg403, Leu597, and the Fe^{3+} shown in sticks and dots. Hydrogen atoms are not shown for clarity.

end of AA with respect to Ile418, when possible, was also taken into account. The models are a solution from F1 [d(C13−OH) = 3.4 Å], from F4 [d(C13−OH) = 4.0 Å], and from F5 [d(C13−OH) = 4.2 Å] and will be referred to as M-F1, M-F4, and M-F5, respectively.

Along these 2 ns MD simulations, some regions of the enzyme show substantial flexibility, especially the α2-, α3-, and α18-helixes (Figure 3). In the M-F4 simulation, there are changes in both the α2- and the α18-helixes: The Leu597 region of the α18-helix is pushed out by AA, making the active site cavity slightly bigger, while the α2-helix closes up a little bit more over the cavity. For the M-F5 simulation, the most significant change occurs at the end of the α18-helix, and it is induced by the positioning of AA during the simulation. Finally, in the M-F1 simulation, the changes with respect to the crystal structure are minor. Keeping in mind that we are looking for precatalytic complexes for hydrogen abstraction at the C13 position, an analysis of the d(H13−OH) distances and the distances representing a possible salt bridge between the AA carboxylate group and the Arg403 was done (see the Supporting Information, Figure S2). Only the M-F4 simulation fulfills both requirements: The interaction with Arg403 is maintained during the whole 2 ns MD simulation, and the d(H13−OH) distances have values short enough to make the reaction plausible. For M-F5, the d(H13−OH) distances become rapidly longer, and the AA carboxylate separates from Arg403, losing this interaction. For M-F1, the interaction with Arg403 is kept during the MD trajectory, but both H13A and H13B go rapidly away from the OH^- moiety once the restraint on d(C13−OH)) is switched off.

Finally, we have run a fourth 2 ns MD simulation starting with a model from family F3 (M-F3), which presents the AA carboxylate buried inside the active site cavity (Figure 2). According to experimental knowledge, this type of complex is not expected to be relevant in 15-rLO, although it is thought to be the main binding mode in other LOs like SLO-1, which presents an Arg residue at the bottom of the cavity. However, the release of the 2P0M crystal structure raised the question of whether the AA could also bind in a horseshoe-like conformation, somewhat resembling the one adopted by RS7 in the ligand-bound monomer.[33] None of the docking poses presents a conformation similar to the one adopted by the inhibitor. However, as indicated above, the docking calculations predicted several solutions with the AA carboxylate positioned close to the polar amino acids around the Fe^{3+} (residues from the first and the second coordination spheres, including Gln548).The MF-3 simulation shows how the AA substrate rotates along the trajectory searching for a polar environment and the final formation of a hydrogen bond between the AA carboxylate and the side chain of His545 (one of the iron ligand residues) (Figure S3 of the Supporting Information). That new AA orientation is not compatible with hydrogen abstractions at C13, although it is interesting because similar interactions seem to be formed also by inhibitors found for 15-hLO.[63] Therefore, the possibility

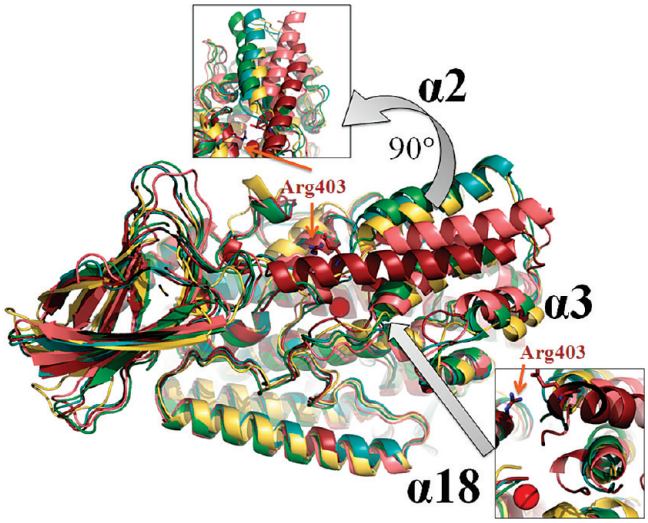

Figure 4. Ligand-free (brown) and ligand-bound (blue) crystal structures and representative structures form the 4 ns MDs of M-F4 (green), M-F4-S (pink), and M-F4-S2 (yellow). The Fe^{3+}, Arg403, and Glu176 of the ligand-free crystal structure are shown as a sphere and in licorice, respectively.

of such interactions, although not relevant for AA reaction, may be an aspect to further consider in the design of 15-LO inhibitors.

Extended MD Simulations of the 15-rLO:AA Complex. From the results of the 2 ns MD simulations, the M-F4 model was selected to pursue the investigation and the modeling of a precatalytic 15-rLO:AA complex. Given the flexibility observed for the enzyme in the available crystal structures and in the MD simulations, we decided to increase the conformational exploration of the system by (1) enlarging the M-F4 simulation up to 4 ns and (2) running two new 4 ns simulations with a slightly different protocol. Those two simulations are referred as M-F4-S and M-F4-S2.

Figure 4 depicts representative structures of the three simulations, together with the two monomers of the crystal structure (ligand-bound and ligand-free). The average Cα−Cα distance between the enzyme:substrate simulations and the ligand-bound crystal structure and between the ligand-bound and ligand-free crystal structures is given in Figure S4 of the Supporting Information. The zones implicated in the conformational change observed between the two crystal structures (α2-, α3-, and α18-helixes) are also flexible zones in our simulations, being the most significant movement that of the α2-helix in simulation M-F4-S. This helix opens up in a way similar to that observed in the crystal structures. Interestingly though, the loop containing residues 171−176 does not get as structured as it does in the experimental ligand-free structure, and the change in the α18-helix is much less pronounced. In the M-F4 and the M-F4-S2 simulations, the big conformational change of the α2-helix was not observed, but both the α2- and the α18-helixes are still flexible. On the other hand, our results also show structural changes in a zone that was not observed to rearrange in the crystal structures. It comprises the α9- and α10-helixes and the loop between them. This zone contains Arg403, Ile418, and Met419.

We have searched for a possible correlation between the movement of the α2- and α18-helixes and the *d*(H13−OH) distance or the interactions made by AA. For the α2-helix, we do not see such a correlation (see Figure S5 in the Supporting Information). The average *d*(H13−OH) distances [in Table S1 of the Supporting Information along with the average *d*(H10−OH) distances] range between 5.52 ± 0.90 (for H13A of M-F4-S2) and 6.49 ± 1.13 Å (for H13A of M-F4-S). Although these average distances are relatively long from the point of view of reactivity, in all of the simulations, much shorter distances are occasionally reached. The results show that the *d*(H13−OH) distances are very sensitive to changes in the AA conformation (see Figure S6 in the Supporting Information). There is no correlation either between the conformation of the α2-helix and the position of AA with respect to the residues situated at the bottom of the cavity (Ile418, Met419, Phe353, and Ile593; see Table S2 in the Supporting Information). In contrast, for the α18-helix, a correlation is observed between its movements and those of the substrate, so that the enzyme adapts to the position of AA.

TABLE 1: Summary of the Interactions Made by the Side Chain of Arg403 in Different Structures and Models Used in This Work[a]

	Ile173	Asp174	Glu176	ligand
2P0M-A	−	−	•	N/A
2P0M-B	•	•	−	−
M-F4	−	−	•	•
M-F4-S	−	−	−	•
M-F4-S2	−	−	•	•
M-F3	•	•	−	−

[a] A dot means that an interaction is present, and a minus sign means the lack of it.

The large displacement of the α2-helix in the M-F4-S simulation is correlated with the hydrogen-bond pattern of Arg403 (Figures 1 and 4). Table 1 summarizes the interactions made by the Arg403 side chain. In the ligand-bound crystal structure, the starting point of our study, the Arg403 side chain is H-bonded to the backbone oxygen of Ile173 and forms a salt bridge with the side chain carboxylate of Asp174. In our simulations, though, the interaction with Ile173 and the salt bridge with Asp174 are broken in all cases (except the simulation in which the AA carboxylate is buried inside the active site cavity, M-F3). Those two interactions are replaced by salt bridges with both the Glu176 and the AA carboxylate groups in the M-F4 and M-F4-S2 simulations. The Glu176−Arg403 interaction was actually present in the ligand-free crystal structure. Interestingly, in the M-F4-S simulation, Arg403 only interacts with the AA and solvent water molecules. Therefore, the change in the H-bond network involving Arg403 could be in the origin of the large α2-helix displacement.

Redocking of AA to 15-rLO Structures from the MD Simulations. The redocking of AA into enzyme structures taken from the 4 ns MD simulations is presented in Table 2. Three structures were taken from each of the M-F4, M-F4-S, and M-F4-S2 simulations. The table also shows the results for the docking of AA into the crystal structure. For each calculation, the number of models out of 100 runs with *d*(C13−OH) < 4.5 Å is given, together with the number of these models that also have the carboxylate of AA at less than 4.0 Å from Arg403. The percentage of models with *d*(C13−OH) < 4.5 Å goes from 12 to 38%. The docking into the crystal structure presents the highest percentage followed by the redockings to M-F4-S snapshots that have percentages between 24 and 31%. When the interaction with Arg403 is also used as a filter, these percentages are reduced to 3−26%. Now, the docking to the crystal structure only produces three positive hits, but in five of the nine snapshots used, there is a great improvement as compared to the use of the crystal structure. In the remaining four cases, the enrichment is small to moderate. Therefore, the

TABLE 2: Summary of the Redocking Results[a]

	C13	C10
M-F4-1	12/4	8/2
M-F4-2	20/18	14/9
M-F4-3	12/7	5/4
M-F4-S-1	29/26	43/34
M-F4-S-2	24/22	29/21
M-F4-S-3	31/25	26/21
M-F4-S2-1	16/6	6/1
M-F4-S2-2	16/5	17/9
M-F4-S2-3	20/16	21/18
crystal structure	38/3	75/8

[a] For each calculation, the number of solutions out of 100 with the distance d(C13-OH) < 4.5 Å is given. The numbers after the slash indicate the solutions that also have the AA carboxylate at less than 4.0 Å of Arg403. The same results are given for the d(C10-OH) distance and for the docking to the crystal structure.

use of several enzyme conformations clearly improves the results, although not all of the individual snapshots represent a clear enrichment. In particular, the M-F4-S redockings maintain most of the solutions (22−26 models) when both filters are applied. For the M-F4 and M-F4-S2 redockings, they both have one case that behaves quite well (around 20% of hits), two of which only represent a small enrichment with respect to the docking to the crystal structure. Besides these geometric filters, which are relatively strict for the present docking calculations, an improvement of the results is also observed in the clustering of the solutions (see the Supporting Information, Figure S7). Overall, there are more populated clusters that have low-energy solutions and, most importantly, present the AA carboxylate in the vicinity of Arg403 and the C13 not too far from the OH^- molecule. It has to be noted, though, that there are still a high number of clusters and a high conformational variability due to the big size of the cavity, the flexibility of the ligand, and the hydrophobicity of the ensemble. Interestingly, a tendency is observed so that the enzyme structures that give a better clustering in the docking calculations are the same that present better precatalytic 15-rLO:AA conformations.

Table 2 also presents the results for the C10 carbon. They are comparable to the ones obtained for C13. The M-F4-S redockings have the highest number of hits. For the crystal structure, when the Arg403 filter is added, the number of hits (which was at 75%) is highly reduced (to 8%). The M-F4 and M-F4-S2 redockings present more variability depending on the enzyme structure, but it seems that an enrichment of the C13 hits is accompanied by an increase in the C10 hits. This is not so strange taking into account the proximity of the two carbon atoms in the AA structure and the cutoff values used as a filter. These results will be further discussed in the next section.

In Silico Mutagenesis. To further analyze the role of Arg403 in AA binding, we have mutated this residue to Ala, Leu, and Lys and performed the docking of AA. This has been done for the nine structures used in the redocking and for the crystal structure. Notice that the Arg403Lys mutation conserves the positive charge, whereas the mutation to Leu or Ala loses the polar character of this residue. The Arg403Ala mutation reduces considerably the size of the side chain. The results have been analyzed in terms of the number of models with d(C13−OH) < 4.5 Å and the number of those models with the AA carboxylate close to the residue 403 (see the Supporting Information, Table S3). If we only consider the d(C13−OH) filter, the results are essentially the same for all of the mutants and for the wild type. Again, the docking calculations show that the active site cavity can accommodate AA with its C13 relatively close to the OH^-. However, when the position of the AA carboxylate is also taken into account, significant differences appear. With Arg and Lys, the results are similar; in most of the models with C13 close to the OH^-, the AA carboxylate interacts with the positively charged residue. With Ala and Leu, the carboxylate is not in the proximity of the mutated position. Moreover, with these neutral residues, a considerable dispersion is observed in the conformations adopted by AA, showing that there are no dominant interactions that can induce a major binding mode. For these mutations, we also observe a displacement of the predicted binding energies to higher values. Contrary, the polar interaction with Lys and Arg results in much better clustered structures and favors a predominant AA orientation. Therefore, although we find 15-rLO:AA complexes with C13 in the vicinity (< 4.5 Å) of the OH^- for all of the mutants, the binding of AA is predicted to be less efficient for the Arg403Ala and Arg403Leu mutants and similar to the wild type enzyme for the Arg403Lys case. These results are in qualitative agreement with the available experimental data. For 15-hLO:AA, in vitro hArg402Leu mutation produced a significant increase in K_M. For the hArg402Lys mutation, the effect was much less pronounced. No significant change was obtained in V_{max}.[24] For rabbit 15-LO, only the effect of the Arg403Leu mutation was experimentally tested and with linoleic acid as a substrate instead of AA; the experiments showed a significant increase in K_M and a lower turnover.[32] Finally, it is interesting to notice that Table S3 in the Supporting Information shows no significant changes for the crystal structure, even when the distance to the mutated residue is added as a filter. The only exception to this would be the Arg403Ala mutation; the AA carboxylate seems to fill the room left by the size reduction of the residue side chain. Again, those results reflect the fact that in the crystal structure Arg403 is not accessible to the substrate.

Discussion

Multiple Binding Modes of AA to 15-rLO. We have performed automated docking calculations to explore the possible binding modes of AA into the ligand-bound crystal structure. The present system is a difficult case for the docking structural search and its limited energy function. As mentioned above and as pointed out by Choi et al.,[33] the cavity to which AA has access is quite big, and AA has a lot of degrees of freedom. This has forced us to use a relatively big spacing for the grid definition, which may have resulted in the loss of some fine-tuning in the energy evaluation. There are also a lot of possible hydrophobic interactions all along the cavity and, in addition, some more localized polar ones. In that sense, our results show that the interactions made in the ligand-bound crystal structure by Arg403 with other residues do not facilitate the anchoring role supposed for this residue; thus, Arg403 does not serve as a major driving force in the docking of AA to this structure. In fact, the docking solutions obey to a shape-solving problem, most of them being in a conformation that simply fills the main cavity (Figure 2). Besides, as the cavity is large, many orientations of the ligand have been obtained, including both methyl end and carboxylate end first poses. It is well-known that for enzymes with a large binding site cavity, docking algorithms generally provide a high variety of orientations. This is not necessarily a problem related to the docking algorithm since one would expect that, at physiological conditions, substantial structural variability would appear in enzymes with a large binding site. For 15-rLO, this is completely coherent with the fact that this enzyme accepts different substrates, indicating a promiscuous binding site[11] and inducing the finding

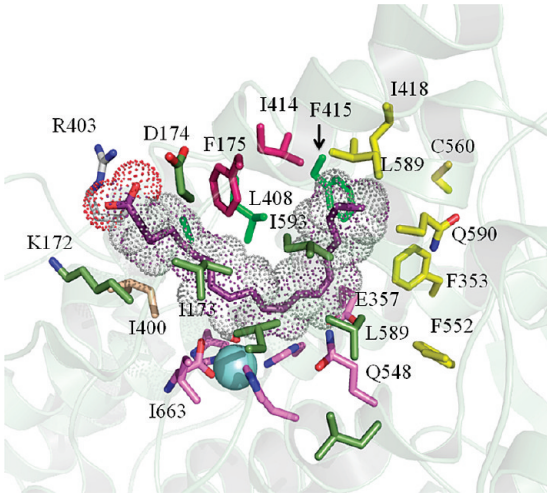

Figure 5. Representation of the active site cavity residues that surround the AA according to the contact analysis. Residues in different zones are depicted in different colors for facilitating visualization. Hydrogen atoms are not shown for clarity.

of several binding modes. Despite this large conformational variability of the 15-rLO:AA complexes, 15-rLO exhibits a high regioselectivity, showing that only a limited part of the conformational space sampled is adequate for catalysis. This subensemble is the focus of our search.

Active Site Cavity and Positioning for Reaction. We have run MD simulations for selected docking solutions to allow the 15-rLO:AA complexes to relax and test their stability. We selected four docking solutions, which included both methyl end and carboxylate end first orientations (from F1, F4, F5, and F3 families; Figure 2). Of the four initial models tested, only the one from the F4 family (model M-F4; Figure S2 in the Supporting Information) produced precatalytic complexes interacting at the same time with Arg403. We have run three different 4 ns trajectories for this F4 model. The results show how AA occupies the cavity described in Gilmor et al.[30,31] (sometimes referred as boot-shaped cavity), which is analogous to the one described for vegetal LOs (although the substrate is in an inverted orientation). A contact analysis along the simulations reveal that AA is well-wrapped by hydrophobic contacts all along the cavity (Figure 5 and Table S4 in the Supporting Information). This cavity is defined (among other residues) by Ile414, Ile418, Met419, Phe353, Leu549, Phe552, Leu589, Ile593, Ile597, and Val594 at the bottom; by Arg403, Ile400, Lys 172, Ile173, Asp174, Phe175, and Glu176 at the entrance extending to the middle; and in the middle part by the iron center and its coordination residues, together with Leu408, Ile597, Gln548, and Glu317. Therefore, it looks like this cavity is optimally prepared for binding the AA. It has to be noticed, though, that there is enough room and side chain flexibility in the cavity to allow some conformational variability in AA, especially for the positioning of the conjugated double bonds and the methyl end. While this article was being written, a work by Neau et al.[64] was published on 8R-LO of *Plexaura homomalla* in which a different cavity is proposed for binding of AA (U-shaped cavity). This cavity does not contemplate a role for Ile418, Met419, or Phe353 as they are not accessible in their ligand-free crystal structures, similar to what is observed in the ligand-free monomer of 15-rLO. They propose a different zone for positioning the methyl end of AA, which would go toward Arg405, Trp145, and Lys146. They also define an important role for the equivalent of Leu408. Although we cannot discard this 8R-LO-derived model, we have to notice that the mutation of the equivalent Leu407 in 15-hLO did not have a significant effect on either the total enzyme activity or the positional specificity.[24] Moreover, and as pointed out recently by Walther et al.,[26] the 8R-LO-derived model does not provide an explanation for the effect produced by the Ile418, Phe353, and Ile593 mutations.

The average d(H13−OH) and some values obtained along the MDs [i.e., d(H13−OH) < 3.0 Å] are consistent with abstraction of H13, especially for H13A. It is interesting to notice that the average d(H13−OH) values for 15-rLO:AA are much longer than the corresponding SLO-1:LA ones. The former values are between 5.52 ± 0.90 (for H13A of M-F4-S2) and 6.49 ± 1.13 Å (for H13A of M-F4-S), while the latter had values for d(C11−-OH) of ∼3.5 Å.[20] This result is consistent with the hydrogen abstraction from AA by 15-rLO being slower (and with less tunneling contribution) than the hydrogen abstraction from LA by SLO-1.

It is also interesting to notice that the docking, the redocking, and the MD results obtained in this work give values for d(C10/H10−OH) comparable to or even shorter than for d(C13/H13−OH). Experimentally, comparable kinetic isotope effects values ($^{D}k_{cat}$[AA]) for abstraction of a hydrogen atom from C13 and C10 of AA were determined by Holman et al.[10,12] in 15-hLO. Moreover, $^{D}k_{cat}/K_{M}$[AA] values of 8 ± 1 and 10 ± 2 (at 22 °C) for abstraction from C13 and C10, respectively, were also determined in the same laboratories.[10,12] According to the authors, the similarity of those C13 and C10 kinetic isotope effects would suggest that the hydrogen atom abstraction at those two structurally distinct positions is of a comparable mechanism and, quite unexpectedly, that the active site of 15-hLO would have to spatially accommodate these two disparate positions for the same hydrogen atom abstraction process. The similar average values obtained for the d(C10/H10−OH) and d(C13/H13−OH) distances in our simulations of the 15-rLO:AA complex reveal that those two carbon atoms are not really in such structurally different locations in a great number of the generated conformations for AA at the active site of 15-rLO. Both carbon atoms can be simultaneously located close enough to the OH^- molecule for the corresponding H-abstraction processes being plausible. Going further, these results could be interpreted as reaction at C10 being not only possible but also faster than reaction at C13, as the C10 hydrogen atoms would be abstracted more easily because they are in fact closer (especially if a tunneling mechanism is expected). However, 15-rLO is known to present a 97:3 ratio for the 15:12 products, so indicating that abstraction at C13 followed by insertion of O_2 at C15 may be the predominant mechanism. Therefore, some other factors than just the initial d(C13/H13−OH) distance might be modulating this regiospecificity. Even though a more complete understanding of the catalytic mechanism will only be possible with the explicit study of the chemical reaction step, a first attempt to explain that apparent contradiction can be given. In most of our simulations, H10 is closer to the oxygen of the OH^- molecule, but its abstraction might be hindered by the OH^- itself. As can be seen in Figure 6 as an illustrative example, the H10 atom is often confronted to the hydrogen atom of OH^-. For the H10 abstraction process to take place resulting in the formation of a water molecule, the H-bond between the OH^- and the carboxylate terminal of Ile663 would need to be broken during the reaction and the H atom of OH^- would need to be rotated. This energy penalty might be high enough to favor abstraction from C13 both in a classical and in a tunneling

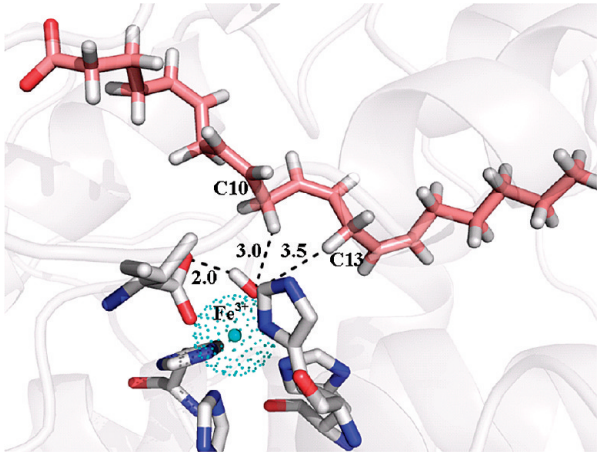

Figure 6. 15-rLO:AA structure taken from the simulations to illustrate one of the dispositions adopted by the H13 and the H10 with respect to the OH^- molecule. Some distances are indicated (in Å), and hydrogen atoms of the protein are not shown for clarity.

mechanism. Besides, the regiospecificity could also be affected by different rates of O_2 attack to the C15 and C12 positions.

Large-Scale Conformational Changes: An Induced-Fit Effect. The results obtained in the three 4 ns trajectories run for the F4 model reflect the significant flexibility of 15-rLO (Figures 4 and S4 and S5 in the Supporting Information), in agreement with the experiments of Kuhn et al.[5] and the conformational changes seen in the crystal structure. Of special relevance is the conformational flexibility of the α2-helix, which in the M-F4-S simulation presents an impressive conformational change. Our analysis suggests that Arg403 and its H-bond pattern may play a key role in the movement of the α2-helix and that the presence of AA disrupting these H-bonds could promote the conformational change. As mentioned above, the entrance to the active site cavity in the ligand-bound crystal structure is somehow hindered due to the interaction of the Arg403 side chain with the Asp174 carboxylate and the backbone carbonyl of Ile173 (Table 1). This feature was neither present in the originally released crystal structure of 15-rLO (1LOX) nor in the ligand-free monomer (2P0M, chain A). In all of our simulations, except the one with the carboxylate buried inside the cavity, the interaction of the Arg403 with Ile173 is lost, and the one with Asp174 is either lost or substituted by a new interaction with the side chain of Glu176, an interaction also observed in the ligand-free monomer (2P0M, chain B) and in the 1LOX crystal structure. Therefore, Arg403 participates in a network of hydrogen bonds at the surface of the protein that change slightly depending on the binding status of the enzyme, that is, if there is a ligand bound or not, how it is bound and the chemical identity of this ligand. It would seem then that in the 15-rLO:RS7 complex, as the inhibitor is far from Arg403, the rearrangement of these H-bonds has produced a structure not optimal for binding of AA. On another side, the simulations have also shown that the looseness of this H-bond network at the base of the α2-helix can be necessary for the large displacement observed for this helix and could be part of the mechanism for opening/closing the α2-helix. Therefore, our calculations reveal that substrate recognition by 15-rLO involves an induced fit effect that might include the breaking of the Arg403 native network of hydrogen bonds to make direct interaction with the substrate. In agreement with the crystal structures, it would be accompanied by a quite global motion of the active site environment. The consideration of these dynamical aspects could improve the drug design process targeting this particular enzyme and probably any mammalian 15-LO.

Impact of Protein Malleability on Catalytic Activity. Kinetic studies predict that prior to hydrogen abstraction, a step involving H-bond rearrangement takes place in the 15-LO:AA reaction. The presence of an effector molecule binding to an allosteric site has been shown to speed up this step. This could be related to the induced effect just mentioned. Thus, our results provide a possible explanation for the mechanism of action of this allosteric effect: The effector molecule disrupts the interactions of the Arg403 side chain and facilitates the conformational change accompanying substrate binding. Meanwhile, we cannot discard the possible involvement of other residues, for example, the H-bond network formed by Glu357, Gln548, and His356 situated inside the active site cavity or the recently suggested His627 and Arg407 residues in epithelial 15-hLO.[9]

Possible implications of Arg403, its network of H-bonds, and the protein flexibility in catalysis also emerge from the redocking calculations. The use of multiple enzyme conformations in the docking process has, in overall, enriched the number of positive hits (that is, 15-rLO:AA complexes with C13 close to the OH^- and the AA carboxylate close to Arg403). Despite the relatively large conformational space explored by AA and the enzyme, only parts of the conformations adopted are reactive. Remarkably, for the structures provided by the M-F4-S simulation, the number of docking solutions with a short d(C13−OH) distance is significantly higher than in any other case, and when the interaction between the substrate and the Arg403 is also used as a filter, most of these M-F4-S solutions remain as positive hits. In the M-F4-S simulation, the Arg403 side chain forms hydrogen bonds with the AA carboxylate but not with the protein. Therefore, it is not surprising that in the redocking calculations a lot of solutions find AA interacting with Arg403. What is significant, though, is that most of these 15-rLO:AA complexes also have the C13 close to the OH^- moiety. This result indicates that the ability of Arg403 to form H-bonds with the AA carboxylate not only favors the conformational change and the binding of AA but also helps the right positioning of C13 for catalysis. The in silico mutagenesis results are also consistent with this hypothesis: The interaction of the AA carboxylate with a polar residue at position 403 induces a predominant orientation of AA in the binding site of 15-rLO. This is expected to be relevant for the correct positioning of AA, not only for proton abstraction at C13 but also for O_2 attack at C15. These observations would also reinforce the idea that the protein malleability contributes to substrate recognition and specificity, as recently suggested by Holman et al.[9,11] for human 15-LO.

Conclusions

We have combined quantum mechanical gas phase calculations, protein−ligand docking, MD simulations, and in silico mutagenesis to study the binding modes of AA to rabbit reticulocyte 15-LO. Our goal has been to find 15-rLO:AA complexes in agreement with the previous mutagenesis experiments and compatible with catalysis. Five major conclusions can be derived from our work. First, AA can bind to 15-rLO in different binding modes, and it fills the boot-shaped cavity. However, only some of these binding solutions are suitable for catalysis, that is, with a short enough C13−OH^- distance. Second, the interaction of the AA carboxylate with Arg403 not only favors binding, but it also modulates a correct positioning for reaction. Third, the

H-bond pattern of Arg403 plays a key role in a α2-helix conformational change observed upon ligand binding. Fourth, the AA can disrupt via an induced-fit effect the above-mentioned interaction pattern and, thus, facilitate the conformational transition. At this point, we can speculate that an effector molecule could have the same effect. Lastly, the crystal coordinates of the inhibitor-bound 15-rLO are not optimal for the binding of AA, essentially because of an inappropriate environment of the Arg403. In that sense, our MD and redocking simulations provide not only a better molecular knowledge on the binding process of AA to 15-rLO but also the grounds for further studies into 15-LO substrate binding and chemical reactivity (which are now in progress in our laboratory) and drug discovery. Likewise, we hope that new experimental data from other laboratories can back up in the near future the theoretical predictions that we have made here.

Acknowledgment. We are thankful for the financial support from the Spanish "Ministerio de Ciencia e Innovación" through projects CTQ2008-02403/BQU and CTQ2008-06866-C02-01 (J.-D.M.), the "Ramon y Cajal" program (L.M.) and consolider-ingenio 2010 no. CSD2007-00006 (J.-D.M.), and "Generalitat de Catalunya" projects 2009SGR409 and 2009SGR68 (J.-D.M.). We are especially grateful to Professor H. Kuhn and Dr. J. Saam for kindly providing us with the force field parameters for the iron and its first coordination sphere ligands.

Supporting Information Available: The clustering histograms of the docking and redocking calculations, distance analysis of the 2 ns MD simulations, structural representations of the simulation with the M-F3 model, average $C_\alpha-C_\alpha$ distances per residue between different structures, distance analysis of the 4 ns MD simulations, depiction of conformations adopted by AA along the simulations, table of the average *d*(H13/10−OH) distances along the 4 ns simulations, table of the distances between AA and selected residues at the bottom of the active site cavity, table of the in silico mutagenesis results, and a table for the contact analysis. This material is available free of charge via the Internet at http://pubs.acs.org.

References and Notes

(1) Kuhn, H. *Prostaglandins, Other Lipid Mediators* **2000**, *62*, 255.
(2) Kuhn, H.; Walther, M.; Kuban, R. J. *Prostaglandins, Other Lipid Mediators* **2002**, *68−69*, 263.
(3) Kuhn, H.; O'Donnell, V. B. *Prog. Lipid Res.* **2006**, *45*, 334.
(4) Walther, M.; Roffeis, J.; Jansen, C.; Anton, M.; Ivanov, I.; Kuhn, H. *Biochim. Biophys. Acta, Mol. Cell Biol. Lipids* **2009**, *1791*, 827.
(5) Mei, G.; Di Venere, A.; Nicolai, E.; Angelucci, C. B.; Ivanov, I.; Sabatucci, A.; Dainese, E.; Kuhn, H.; Maccarrone, M. *Biochemistry* **2008**, *47*, 9234.
(6) Saam, J.; Ivanov, I.; Walther, M.; Holzhutter, H. G.; Kuhn, H. *Proc. Natl. Acad. Sci. U.S.A.* **2007**, *104*, 13319.
(7) Romanov, S.; Wiesner, R.; Myagkova, G.; Kuhn, H.; Ivanov, I. *Biochemistry* **2006**, *45*, 3554.
(8) Ivanov, I.; Romanov, S.; Ozdoba, C.; Holzhutter, H. G.; Myagkova, G.; Kuhn, H. *Biochemistry* **2004**, *43*, 15720.
(9) Wecksler, A. T.; Kenyon, V.; Garcia, N. K.; Deschamps, J. D.; van der Donk, W. A.; Holman, T. R. *Biochemistry* **2009**, *48*, 8721.
(10) Wecksler, A. T.; Jacquot, C.; van der Donk, W. A.; Holman, T. R. *Biochemistry* **2009**, *48*, 6259.
(11) Wecksler, A. T.; Kenyon, V.; Deschamps, J. D.; Holman, T. R. *Biochemistry* **2008**, *47*, 7364.
(12) Jacquot, C.; Wecksler, A. T.; McGinley, C. M.; Segraves, E. N.; Holman, T. R.; van der Donk, W. A. *Biochemistry* **2008**, *47*, 7295.
(13) Segraves, E. N.; Holman, T. R. *Biochemistry* **2003**, *42*, 5236.
(14) Glickman, M. H.; Klinman, J. P. *Biochemistry* **1995**, *34*, 14077.
(15) Glickman, M. H.; Klinman, J. P. *Biochemistry* **1996**, *35*, 12882.
(16) Lehnert, N.; Solomon, E. I. *J. Biol. Inorg. Chem.* **2003**, *8*, 294.
(17) McGinley, C. M.; van der Donk, W. A. *Chem. Commun.* **2003**, 2843.
(18) Lewis, E. R.; Johansen, E.; Holman, T. R. *J. Am. Chem. Soc.* **1999**, *121*, 1395.
(19) Kohen, A.; Klinman, J. P. *Acc. Chem. Res.* **1998**, *31*, 397.
(20) Tejero, I.; Garcia-Viloca, M.; González-Lafont, À.; Lluch, J. M.; York, D. M. *J. Phys. Chem. B* **2006**, *110*, 24708.
(21) Jacquot, C.; Peng, S.; van der Donk, W. A. *Bioorg. Med. Chem. Lett.* **2008**, *18*, 5959.
(22) Knapp, M. J.; Klinman, J. P. *Biochemistry* **2003**, *42*, 11466.
(23) Schneider, C.; Pratt, D. A.; Porter, N. A.; Brash, A. R. *Chem. Biol.* **2007**, *14*, 473.
(24) Gan, Q. F.; Browner, M. F.; Sloane, D. L.; Sigal, E. *J. Biol. Chem.* **1996**, *271*, 25412.
(25) Borngraber, S.; Browner, M.; Gillmor, S.; Gerth, C.; Anton, M.; Fletterick, R.; Kuhn, H. *J. Biol. Chem.* **1999**, *274*, 37345.
(26) Vogel, R.; Jansen, C.; Roffeis, J.; Reddanna, P.; Forsell, P.; Claesson, H.-E.; Kuhn, H.; Walther, M. *J. Biol. Chem.* **2010**, *285*, 5369.
(27) Sloane, D. L.; Leung, R.; Craik, C. S.; Sigal, E. *Nature* **1991**, *354*, 149.
(28) Chen, X. S.; Funk, C. D. *FASEB J.* **1993**, *7*, 694.
(29) Borngraber, S.; Kuban, R. J.; Anton, M.; Kuhn, H. *J. Mol. Biol.* **1996**, *264*, 1145.
(30) Gillmor, S. A.; Villasenor, A.; Fletterick, R.; Sigal, E.; Browner, M. F. *Nat. Struct. Biol.* **1997**, *4*, 1003.
(31) Gillmor, S. A.; Villasenor, A.; Fletterick, R.; Sigal, E.; Browner, M. F. *Nat. Struct. Biol.* **1998**, *5*, 242.
(32) Schwarz, K.; Borngraber, S.; Anton, M.; Kuhn, H. *Biochemistry* **1998**, *37*, 15327.
(33) Choi, J.; Chon, J. K.; Kim, S.; Shin, W. *Proteins: Struct., Funct., Bioinf.* **2008**, *70*, 1023.
(34) Falgueyret, J. P.; Denis, D.; Macdonald, D.; Hutchinson, J. H.; Riendeau, D. *Biochemistry* **1995**, *34*, 13603.
(35) Holman, T. R.; Mogul, R.; Johansen, E. *Biochemistry* **2000**, *39*, 1545.
(36) Mogul, R.; Johansen, E.; Holman, T. R. *Biochemistry* **2000**, *39*, 1544.
(37) Schames, J. R.; Henchman, R. H.; Siegel, J. S.; Sotriffer, C. A.; Ni, H. H.; McCammon, J. A. *J. Med. Chem.* **2004**, *47*, 1879.
(38) Amaro, R. E.; Baron, R.; McCammon, J. A. *J. Comput.-Aided Mol. Des.* **2008**, *22*, 693.
(39) Amaro, R. E.; Schnaufer, A.; Interthal, H.; Hol, W.; Stuart, K. D.; McCammon, J. A. *Proc. Natl. Acad. Sci. U.S.A.* **2008**, *105*, 17278.
(40) Hritz, J.; de Ruiter, A.; Ostenbrink, C. *J. Med. Chem.* **2008**, *51*, 7469.
(41) Degliesposti, G.; Kasam, V.; Da Costa, A.; Kang, H. K.; Kim, N.; Kim, D. W.; Breton, V.; Kim, D.; Rastelli, G. *ChemMedChem* **2009**, *4*, 1164.
(42) Alonso, H.; Bliznyuk, A. A.; Gready, J. E. *Med. Res. Rev.* **2006**, *26*, 531.
(43) Morris, G. M.; Huey, R.; Lindstrom, W.; Sanner, M. F.; Belew, R. K.; Goodsell, D. S.; Olson, A. J. *J. Comput. Chem.* **2009**, *30*, 2785.
(44) Huey, R.; Morris, G. M.; Olson, A. J.; Goodsell, D. S. *J. Comput. Chem.* **2007**, *28*, 1145.
(45) Li, H.; Robertson, A. D.; Jensen, J. H. *Proteins: Struct., Funct., Bioinf.* **2005**, *61*, 704.
(46) Dolinsky, T. J.; Czodrowski, P.; Li, H.; Nielsen, J. E.; Jensen, J. H.; Klebe, G.; Baker, N. A. *Nucleic Acids Res.* **2007**, *35*, W522.
(47) Sanner, M. F. *Structure* **2005**, *13*, 447.
(48) Bayly, C. I.; Cieplak, P.; Cornell, W. D.; Kollman, P. A. *J. Phys. Chem.* **1993**, *97*, 10269.
(49) Hay, P. J.; Wadt, W. R. *J. Chem. Phys.* **1985**, *82*, 270.
(50) Hay, P. J.; Wadt, W. R. *J. Chem. Phys.* **1985**, *82*, 299.
(51) Zhao, Y.; Schultz, N. E.; Truhlar, D. G. *J. Chem. Theory Comput.* **2006**, *2*, 364.
(52) Reed, A. E.; Weinstock, R. B.; Weinhold, F. *J. Chem. Phys.* **1985**, *83*, 735.
(53) Brooks, B. R.; Bruccoleri, R. E.; Olafson, B. D.; States, D. J.; Swaminathan, S.; Karplus, M. *J. Comput. Chem.* **1983**, *4*, 187.
(54) Brooks, B. R.; Brooks, C. L.; Mackerell, A. D.; Nilsson, L.; Petrella, R. J.; Roux, B.; Won, Y.; Archontis, G.; Bartels, C.; Boresch, S.; Caflisch, A.; Caves, L.; Cui, Q.; Dinner, A. R.; Feig, M.; Fischer, S.; Gao, J.; Hodoscek, M.; Im, W.; Kuczera, K.; Lazaridis, T.; Ma, J.; Ovchinnikov, V.; Paci, E.; Pastor, R. W.; Post, C. B.; Pu, J. Z.; Schaefer, M.; Tidor, B.; Venable, R. M.; Woodcock, H. L.; Wu, X.; Yang, W.; York, D. M.; Karplus, M. *J. Comput. Chem.* **2009**, *30*, 1545.
(55) Hoover, W. G. *Phys. Rev. A* **1985**, *31*, 1695.
(56) Ryckaert, J. P.; Ciccotti, G.; Berendsen, H. J. C. *J. Comput. Phys.* **1977**, *23*, 327.
(57) Feller, S. E.; MacKerell, A. D. *J. Phys. Chem. B* **2000**, *104*, 7510.
(58) Feller, S. E.; Gawrisch, K.; MacKerell, A. D. *J. Am. Chem. Soc.* **2002**, *124*, 318.
(59) MacKerell, A. D.; Feig, M.; Brooks, C. L. *J. Comput. Chem.* **2004**, *25*, 1400.

(60) MacKerell, A. D.; Bashford, D.; Bellott, M.; Dunbrack, R. L.; Evanseck, J. D.; Field, M. J.; Fischer, S.; Gao, J.; Guo, H.; Ha, S.; Joseph-McCarthy, D.; Kuchnir, L.; Kuczera, K.; Lau, F. T. K.; Mattos, C.; Michnick, S.; Ngo, T.; Nguyen, D. T.; Prodhom, B.; Reiher, W. E.; Roux, B.; Schlenkrich, M.; Smith, J. C.; Stote, R.; Straub, J.; Watanabe, M.; Wiorkiewicz-Kuczera, J.; Yin, D.; Karplus, M. *J. Phys. Chem. B* **1998**, *102*, 3586.

(61) Pettersen, E. F.; Goddard, T. D.; Huang, C. C.; Couch, G. S.; Greenblatt, D. M.; Meng, E. C.; Ferrin, T. E. *J. Comput. Chem.* **2004**, *25*, 1605.

(62) Schenk, G.; Neidig, M. L.; Zhou, J.; Holman, T. R.; Solomon, E. I. *Biochemistry* **2003**, *42*, 7294.

(63) Kenyon, V.; Chorny, I.; Carvajal, W. J.; Holman, T. R.; Jacobson, M. P. *J. Med. Chem.* **2006**, *49*, 1356.

(64) Neau, D. B.; Gilbert, N. C.; Bartlett, S. G.; Boeglin, W.; Brash, A. R.; Newcomer, M. E. *Biochemistry* **2009**, *48*, 7906.

JP912120N